On the channel estimation of low-PAPR waveform for 5G Evolution and 6G

Lijun Yang[1], Lilin Dan[1], Yuanjie Hu[1], Ping Yang[1], Saviour Zammit[2]
[1]*National Key Laboratory of Wireless Communications*
University of Electronic Science and Technology of China, Chengdu, China
[2]*Department of Communications and Computer Engineering*
University of Malta, Msida, Malta
Email: lilindan@uestc.edu.cn

***Abstract*—In order to mitigate the high peak-to-average power ratio (PAPR) of the uplink waveform, the frequency domain spectrum shaping (FDSS) and $\frac{\pi}{2}$ BPSK modulation are adopted to DFT spread orthogonal frequency-division multiplexing (DFT-s-OFDM) for both data and pilot transmission in 5G new radio (NR). However, generating such pilot sequences with acceptable orthogonality and reduced PAPR causes a computationally intensive search. This paper introduces the constant envelope (CE) OFDM waveform for both pilot and data transmitting with a PAPR of 0dB. Especially, an modified channel estimation scheme with the optimized selection of modulation index is proposed to overcome the non-flat power spectral density caused by phase modulation in CE-OFDM. Numerical results prove the superiority of the proposed low-PAPR waveform over the classical NR signal in terms of both PAPR and BER performance.**

***Index Terms*—PAPR, OFDM, constant envelope, channel estimation**

I. Introduction

As a result of the high frequency transmission characteristics and terminal transmit power limitations of the fifth generation (5G), the uplink coverage of 5G cells is more limited [2], and the design of low peak-to-average-power-ratio (PAPR) waveform, encompassing both pilot signal and data signal, has become a significant research focus [1].

In order to address the high PAPR of orthogonal frequency-division multiplexing (OFDM) waveform and enhance the cell coverage of 5G new radio (NR), the 3GPP standard introduces a new modulation scheme, i.e., $\frac{\pi}{2}$ BPSK, for uplink data and control channel transmissions [3]. By combining this with DFT spreading [4] and frequency domain spectrum shaping (FDSS) [5], low PAPR transmission can be achieved. However, the use of zaddoff chu (ZC)-based pilot sequences in conventional uplink transmission, which are essential for coherent detection, still poses limitations on cell coverage due to their variously high PAPR. To address the PAPR variability of pilot signal, DFT-s-OFDM waveform combined with $\frac{\pi}{2}$ BPSK and FDSS is also adopted for pilot transmission in NR Release 17 [6], [7]. However, the $\frac{\pi}{2}$ BPSK-based low-PAPR pilot signal requires a complicated search to obtain sequences with good correlation and low PAPR, especially for sequences with the length longer than 30. On the other hand, the channel estimation performance for cell edge users can be improved by power boosting the pilot sequence, which is only possible when the pilot sequence has a PAPR as low as possible [8]. Therefore finding sequences with lower PAPR needs to be further considered for 5G evolution and beyond.

The work was supported by National Science Foundation of China under Grant number 62071111 and the Fundamental Research Funds for the Central Universities under Grant 2242022k6006.

Constant envelop OFDM (CE-OFDM) technique utilizes the phase information of a constant envelope signal to embed the high-PAPR OFDM signal [9], which leads to a PAPR of 0 dB. Unlike traditional single-carrier system, CE-OFDM can easily allocate available subcarriers to different users [10], which is friendly to frequency domain resource scheduling like the OFDM-based system. Moveover, researches have shown that compared to OFDM, CE-OFDM exhibits superior bit error rate (BER) performance and coverage range in scenarios with significant attenuation [10], [11]. However, the existing channel estimation techniques designed for OFDM is not suitable for CE-OFDM, since the non-linear operation of phase modulation lead a non-uniform power distribution in frequency domain. Therefore, the conventional pilot-aided CE-OFDM scheme still suffers from high PAPR by utilizing OFDM signal and ZC sequence for channel estimation [12].

Building upon the advantage of 0dB PAPR performance, this paper considers CE-OFDM signal for both pilot and data transmission toward 5G evolution and beyond. Additionally, a modified channel estimation scheme is proposed based on the justified signal-to-noise distribution and the optimized selection of modulation index. Finally, via computer simulations, it has been shown that CE-OFDM signals exhibited superior PAPR and BER performance,compared to the existing 5G NR lower-PAPR waveforms.

The remainder of this paper is organized as follows. Section II introduces the conventional low-PAPR waveform and pilot design in current 5G NR standard. Section III presents the proposed low-PAPR transmitting and channel estimation scheme based on CE-OFDM, following by the numeric simulation and conclusion in section IV and section V, respectively.

II. Pilot-aided Low-PAPR transmission in 5G NR

In this section, we introduce the low PAPR transmission scheme in 5G NR uplink. When $\frac{\pi}{2}$ BPSK modulation combined with spectral shaping [5] and transform precoding [3],

979-8-3503-2928-5/23/$31.00 ©2023 IEEE

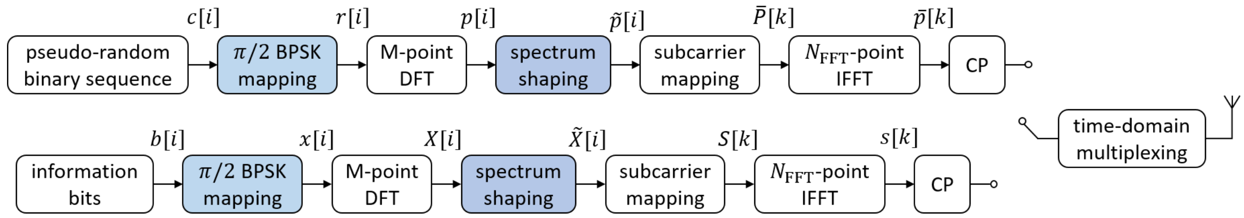

(a) The structure of $\frac{\pi}{2}$ BPSK DFT-s-OFDM waveform with pilot based on $\frac{\pi}{2}$ BPSK modulation.

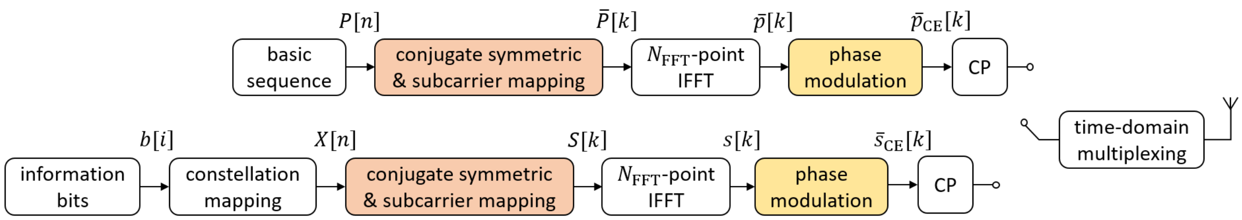

(b) The structure of CE-OFDM waveform with pilot based on CE-OFDM modulation.

Fig. 1. The structures of the two waveforms: (a) $\frac{\pi}{2}$ BPSK DFT-s-OFDM modulation; (b) CE-OFDM modulation.

which is realized by the DFT spreading (DFT-s), it can achieve a PAPR performance of up to 2dB lower than conventional OFDM signals. On the other hand, the ZC pilot sequence, which is commonly used to obtain channel state information (CSI) at the receiver, has a high PAPR. To match the PAPR of the data signals, a corresponding approach is proposed, which utilizes a pilot sequence based on $\frac{\pi}{2}$ BPSK modulation [3]. As a result, both the data and pilot transmission have the same PAPR.

Fig. 1(a) illustrates the system of $\frac{\pi}{2}$ BPSK FDSS-DFT-s-OFDM waveform with the pilot sequence based with $\frac{\pi}{2}$ BPSK. The pilot signal and data signal are multiplexed in the time domain, therefore the frequency channel estimation and equalization is applied at the receiver side. Since the same waveform scheme is applied to data symbols and pilot symbols, we mainly describe the pilot sequence generation process for simplification.

As specified in TS 38.211 Section 5.2.1 [3], we first perform $\frac{\pi}{2}$ BPSK mapping on a pseudo-random binary sequence (PRBS) $c[i](i=0,1,\cdots,N-1)$ to obtain the modulation symbol $r[i](i=0,1,\cdots,N-1)$, which is mapped as

$$r[i]=\frac{e^{j\frac{\pi}{2}(i\mathrm{mod}2)}}{\sqrt{2}}[(1-2c[i])+j(1-2c[i])]. \tag{1}$$

After an N-point DFT on $r[i]$, the resultant frequency-domain signal $p[i](i=0,1,\cdots,N-1)$ is applied to spectrum shaping, obtaining $\tilde{p}[i]$ according to

$$\tilde{p}[i]=p[i]s_{0.28}[i], i=0,1,\cdots,N-1. \tag{2}$$

Here, $\mathbf{s}_{0.28}$ is a filter tap vector of length N that

$$\mathbf{s}_{0.28}=\mathbf{W}_N[1,-0.28,\mathbf{0}_{N-3},-0.28]^{\mathrm{T}}, \tag{3}$$

where $\mathbf{W}_N$ is the DFT transform matrix expressed as

$$[\mathbf{W}_N]_{(i,j)}=\frac{1}{\sqrt{N}}e^{-j\frac{2\pi}{N}(i-1)(j-1)}, i,j=1,2,\cdots,N. \tag{4}$$

Then, the shaped sequence $\tilde{\mathbf{p}}$ with length N is mapped onto N_{FFT} subcarriers to obtain $\bar{P}[k], k=0,1,\cdots,N_{\mathrm{FFT}}$. Finally applying N_{FFT}-point inverse Fast Fourier Transform (IFFT) transformation, we can obtain $\frac{\pi}{2}$-BPSK-based low-PAPR sequence $\bar{\mathbf{p}}$. Since both the pilot sequence and data are generated using $\frac{\pi}{2}$ BPSK and FDSS-DFT-s-OFDM, their PAPR are effectively the same.

At the receiver, conventional channel estimation methods such as least square (LS) and minimum mean square error (MMSE) can be employed to obtain CSI. Subsequently, channel equalization and demodulation are performed to recover the transmitted data bits as described in [13].

III. Proposed Lowe-PAPR transmission based on CE-OFDM

A. *Transmitter structure*

Despite the lower PAPR achieved by $\frac{\pi}{2}$ BPSK sequences comparing to the conventional OFDM signal, channel estimation performance for cell edge users requires a pilot sequence as low as possible. In contrast, CE-OFDM technique embeds high-PAPR OFDM symbols into the phase information, theoretically resulting in transmitted waveform with a PAPR of 0dB. However, in previous research, the conventional pilot signals, such as OFDM and ZC sequence, are adopted for CE-OFDM system, since the impairment of non-uniform power distribution of CE-OFDM symbols and the uniform single-to-noise assumption in the conventional OFDM-based channel estimation schemes. To address this issue, this study proposes modified channel estimation scheme for the simultaneous use of CE-OFDM as pilot sequences and data waveform.

Fig. 1(b) illustrates the time-domain multiplexing structure of pilot-aided CE-OFDM system. For the case of CE-OFDM pilot sequence, a basic signal sequences $\mathbf{P}=[P(0),P(1),\cdots,P(\frac{N}{2}-2)]$, such as ZC sequences is firstly generated in the frequency domain. In order to obtain the real-valued time-domain sequence, $\bar{\mathbf{P}}$ need to satisfy the conjugate-symmetry structure by performing conjugate symmetry and subcarrier mapping as

$$\bar{\mathbf{P}} = [0, P(0), \cdots, P(\frac{N}{2}-2), \mathbf{0}_{\mathrm{ZP}}, 0, P^*(\frac{N}{2}-2), \cdots, P^*(0)], \tag{5}$$

where the length of $\bar{\mathbf{P}}$ is N_{FFT}. Then, perform N_{FFT}-point IFFT to $\bar{\mathbf{P}}$ and obtain time domain signal $\bar{\mathbf{p}}$. To obtain the CE-OFDM sequence $\bar{\mathbf{p}}_{\mathrm{CE}}$ with 0dB PAPR, we then perform phase modulation to $\bar{\mathbf{p}}$, as shown in (6):

$$\bar{\mathbf{p}}_{\mathrm{CE}} = Aexp\{j2\pi h C_N . * \bar{\mathbf{p}}\}, \tag{6}$$

where A is the amplitude scalar, $2\pi h$ is the modulation index and C_N is the normalization factor. To ensure the variance of the signal phase $\phi = 2\pi h C_N . * \bar{\mathbf{p}}$ to be $(2\pi h)^2$, the normalization constant factor C_N is given by

$$C_N = \sqrt{(N_{\mathrm{FFT}})^2/[(N-2)]}. \tag{7}$$

B. Receiver with the improved MMSE channel estimation

Since the receiver needs to perform channel equalization and coherence detection to recover the transmitted bits, channel estimation assisted with the pilot sequence is required to obtain CSI. Due to the non-linear nature of phase modulation/demoduation, the CE-OFDM pilot sequence, despite its advantage of constant envelope, exhibits an non-uniform power distribution in the frequency domain. Consequently, this inconsistency leads to non-identical carrier-to-noise-ratio (CNR), resulting in varied channel estimation performance among subcarriers.

In this section, we present a improved MMSE channel estimation scheme for the receiver of CE-OFDM system. Taking into account the influence of noise based on the principles of the MMSE algorithm, we modify the signal-to-noise ratio (SNR) at each subcarrier in the correlation matrix calculation, considering the energy distribution of the CE-OFDM pilot sequence in the frequency domain. This optimization aims to enhance the channel estimation performance of the CE-OFDM pilot sequence.

Assume that the received signal is represented as

$$\mathbf{Y} = \mathbf{H}\bar{\mathbf{P}}_{\mathrm{CE}} + \mathbf{N}, \tag{8}$$

where $\mathbf{Y}$ is the received signal, $\mathbf{H}$ is the frequency domain channel matrix, and $\mathbf{N}$ is additive Gaussian noise, obeying $\mathcal{CN}(0, N_0)$.

In order to perform channel estimation in frequency domain at the receiver, we utilize FFT to transform the acquired time-domain pilot sequence $\bar{\mathbf{p}}_{\mathrm{CE}}$ into the frequency domain. This process finally enables to obtain the frequency domain pilot sequence $\bar{\mathbf{P}}_{\mathrm{CE}}$ with a length of N_{FFT}. For the uneven energy distribution in the frequency domain of CE-OFDM signals, we optimize the MMSE channel estimation results by compensating the energy of each subcarrier when calculating the weighting matrix at the receiver side. The specific implementation steps are:

Step 1: LS channel estimation. First, we obtain the LS channel estimation by the following equation:

$$\tilde{\mathbf{H}} = \bar{\mathbf{P}}_{\mathrm{CE}}^{-1}\mathbf{Y}. \tag{9}$$

Step 2: Compute the weight matrix $\mathbf{W}$. According to [14], the weight matrix for MMSE channel estimation is given by the following expression:

$$\mathbf{W} = \mathbf{R}_{\mathbf{H}\tilde{\mathbf{H}}}(\mathbf{R}_{\mathbf{HH}} + \frac{1}{snr}\mathbf{I})^{-1}, \tag{10}$$

where $\mathbf{R}_{\mathbf{H}\tilde{\mathbf{H}}}$ denotes the correlation matrix between the real channel vector and the LS channel estimation vector in the frequency domain, while $\mathbf{R}_{\mathbf{HH}}$ represents the auto-correlation matrix of the real channel vector. Since the CE-OFDM sequence has uneven energy distribution across subcarriers, in order to correct the snr on each subcarrier, we modify the weight matrix as shown in (11):

$$\mathbf{W}_{\mathrm{improved}} = \mathbf{R}_{\mathbf{H}\tilde{\mathbf{H}}}(\mathbf{R}_{\mathbf{HH}} + \boldsymbol{\beta}. * \frac{1}{snr}\mathbf{I})^{-1}, \tag{11}$$

where the vector of correction coefficients $\boldsymbol{\beta}$ is computed as:

$$\beta[n] = \frac{1}{|\bar{\mathbf{P}}_{\mathrm{CE}}[n]|^2}, n = 1, 2, \cdots, N_{\mathrm{FFT}}. \tag{12}$$

Step 3: MMSE channel estimation. Based on the weight matrix $\mathbf{W}_{\mathrm{improved}}$ and the LS channel estimation $\tilde{\mathbf{H}}$, we finally obtain the MMSE channel estimation as follows

$$\hat{\mathbf{H}} = \mathbf{W}_{\mathrm{improved}}\tilde{\mathbf{H}}. \tag{13}$$

After obtaining the estimated channel information $\hat{\mathbf{H}}$, we perform maximum likelihood (ML) detection to recover the transmitted CE-OFDM symbols [15] following

$$\hat{\mathbf{S}} = \underset{\mathbf{S}\in\Omega}{\mathrm{argmin}}||\mathbf{Y} - \hat{\mathbf{H}} \cdot \mathrm{FFT}[\mathrm{e}^{\mathrm{j}2\pi\mathrm{hC_N}\cdot\mathrm{IFFT}[\mathbf{S}]}]||^2, \tag{14}$$

where Ω represents the set of all possible frequency-domain modulation symbols.

IV. SIMULATION RESULTS

In this section, we conducted simulations on the proposed pilot-aided CE-OFDM transmission. The simulations were performed using the fading channel of Extended Vehicular A model (EVA), which is with 9-path Rayleigh channel [16]. For all the system, the MMSE algorithm was utilized for channel estimation at the receiver. For the $\frac{\pi}{2}$BPSK-aided DFT-s-OFDM and the CE-OFDM transmission, $\frac{\pi}{2}$BPSK sequence and CE-OFDM sequence are generated as the reference pilot for channel estimation, respectively. All the transmission are configured with $N_{\mathrm{FFT}} = 256$ subcarriers.

In Fig. 2, we compared the PAPR performance of pilot sequences utilizing ZC sequences, $\frac{\pi}{2}$BPSK sequences, and CE-OFDM sequences, respectively. The sequence length is 128, and the FFT size is 1024. The graph shows the PAPR for both filtered and unfiltered cases, marked as with and without FDSS, respectively. As can be seen from the figure, applying FDSS to the conventional OFDM-based low-PAPR pilot sequence, i.e., the ZC sequence and the $\frac{\pi}{2}$BPSK-modulated sequence, achieves different PAPR performance. At the complementary cumulative distribution function (CCDF) of 10^{-3}, the PAPR of the unfiltered ZC sequence and $\frac{\pi}{2}$BPSK sequence is 2.9dB higher than that of the $\frac{\pi}{2}$BPSK pilot sequence with FDSS. Furthermore, the PAPR of the filtered

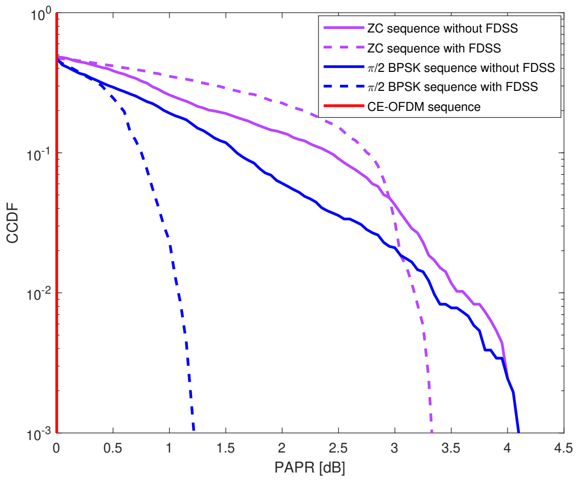

Fig. 2. PAPR comparison among pilot signal using $\frac{\pi}{2}$BPSK-DFT-s-OFDM, ZC and CE-OFDM sequence.

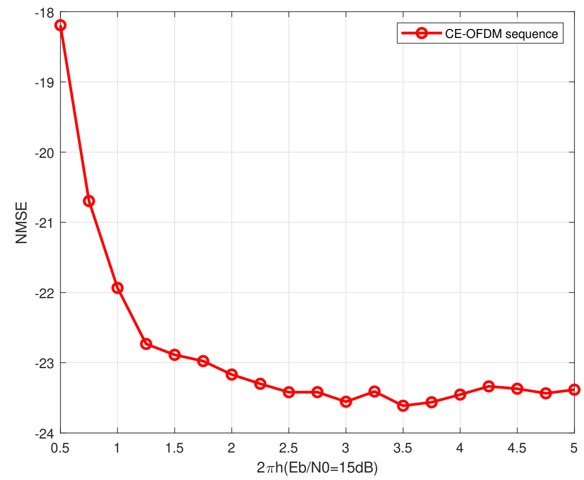

Fig. 4. NMSE performance of channel estimation at different values of $2\pi h$ (E_b/N_0 = 15dB).

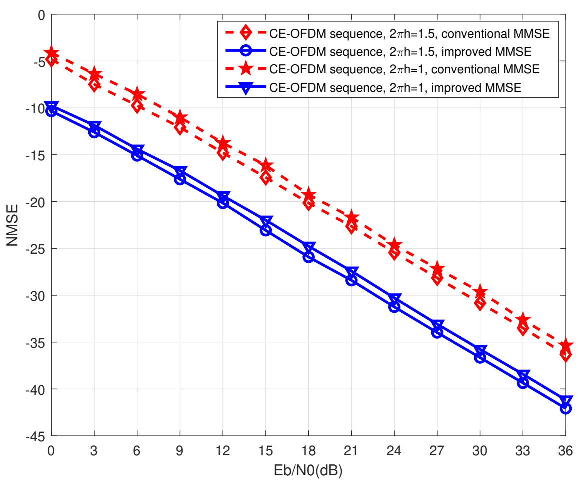

Fig. 3. NMSE comparison among conventional MMSE and improved MMSE of CE-OFDM sequences.

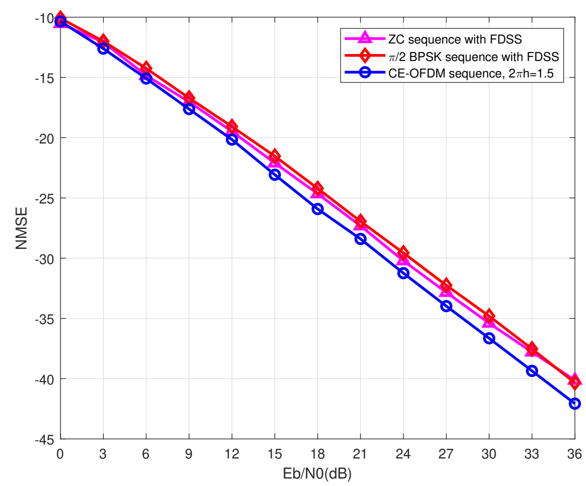

Fig. 5. NMSE comparison among ZC, $\frac{\pi}{2}$ BPSK with FDSS and CE-OFDM sequences.

ZC sequence is still about 2.1dB higher than that of the $\frac{\pi}{2}$ BPSK sequence with the same FDSS. On the other hand, the CE-OFDM pilot sequence has a constant envelope property, resulting in a 0dB PAPR. In this case, the PAPR of the $\frac{\pi}{2}$ BPSK pilot sequence with FDSS is about 1.2dB higher than that of the CE-OFDM pilot sequence. Considering all aspects, the CE-OFDM sequence demonstrates an absolute advantage in terms of PAPR performance.

Fig. 3 shows the normalized mean square error (NMSE) comparison of channel estimation between conventional MMSE channel estimation and improved MMSE channel estimation when using CE-OFDM pilot sequence. The modulation index of the CE-OFDM pilot sequence is set as $2\pi h = 1$ and $2\pi h = 1.5$. It can be observed that, at the NMSE of -30dB, the proposed improved MMSE channel estimation achieves a gain of approximately 6.5dB compared to the conventional channel estimation algorithm, greatly improving the channel estimation performance of the CE-OFDM sequence.

In Fig. 4, we compare the channel estimation performance of CE-OFDM pilot sequences under different values of modulation index $2\pi h$. The simulations are conducted with $E_b/N_0 = 15$dB. Upon observing the curve, it is evident that for smaller values of $2\pi h$, where $2\pi h < 1.25$, the channel estimation error is more significant. However, as the modulation index $2\pi h$ exceeds 1.5, the range of fluctuations in channel estimation error reduces. Due to the significant signal leakage out-of-band caused by a larger value of $2\pi h$, we made a compromise in our subsequent simulations by setting $2\pi h = 1.5$.

In Fig. 5, we compared the NMSE performance of three types of pilot sequences. The ZC sequence and $\frac{\pi}{2}$ BPSK sequence undergo spectrum shaping to reduce the PAPR of the time-domain waveform. By comparing the curves in Fig. 5, it can be seen that the channel estimation performance of the ZC sequence and $\frac{\pi}{2}$ BPSK pilot sequence is similar. However, at the NMSE of -40dB, the CE-OFDM sequence achieves a performance gain of approximately 2dB compared to the other two sequences. Therefore, compared to ZC and $\frac{\pi}{2}$ BPSK pilot sequences, the CE-OFDM pilot sequence not only provides the advantage of 0dB PAPR but also maintains excellent channel estimation performance.

In Fig. 6, we present the simulated BER performance of

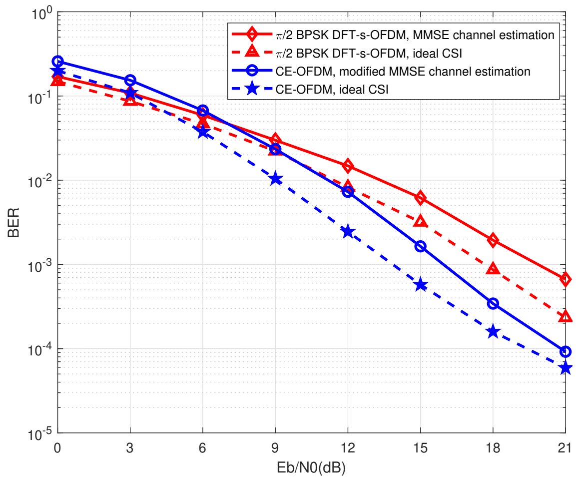

Fig. 6. BER comparison among $\frac{\pi}{2}$ BPSK DFT-s-OFDM and CE-OFDM systems with ideal CSI and assisted with $\frac{\pi}{2}$ BPSK sequence and CE-OFDM sequence, respectively.

$\frac{\pi}{2}$ BPSK DFT-s-OFDM and CE-OFDM waveforms, where both waveforms are utilized as pilot and data signals simultaneously. We evaluate the BER performance with two scenarios: channel estimation assisted with pilot signals and under ideal CSI. The CE-OFDM signal is demodulated using ML demodulation. The system employs a total of $N_{\mathrm{FFT}} = 32$ subcarriers. By comparing the BER curves of CE-OFDM and $\frac{\pi}{2}$BPSK DFT-s-OFDM under ideal CSI, we observe that the BER of $\frac{\pi}{2}$ BPSK DFT-s-OFDM outperforms CE-OFDM at $E_b/N_0 < 6$dB. However, at high SNRs, CE-OFDM demonstrates higher diversity gain, resulting in improved BER performance. A similar conclusion can be drawn when comparing the BER under real channel estimation. Therefore, it can be concluded that CE-OFDM achieves better BER performance without compromising channel estimation accuracy when used as both the pilot and data waveforms, compared to the $\frac{\pi}{2}$ BPSK DFT-s-OFDM waveform.

V. Conclusions

In this paper, we proposed a novel scheme for generating lower PAPR waveform for both pilot and data symbols. By employing phase modulation and time-domain multiplexing, we achieved a whole CE-OFDM waveform with 0dB PAPR. Furthermore, considering the non-flat power distribution in the frequency domain of CE-OFDM pilot sequence, we developed an improved MMSE channel estimation that optimized the estimation performance. Finally, via computer simulations, it has been shown that compared to the conventional 5G NR lower-PAPR waveform, CE-OFDM signals exhibited superior PAPR and channel estimation performance. Additionally, to maintain consistency between pilot and data PAPR, we further simulated the system BER with CE-OFDM waveforms serving as both pilot and data signals. In high SNR regions, CE-OFDM waveforms demonstrated better BER performance.

References

[1] Z. Guo, D. Chen and Y. Yuan, ”5G NR Uplink Coverage Enhancement Based on DMRS Bundling and Multi-slot Transmission,” 2020 IEEE 20th International Conference on Communication Technology (ICCT), Nanning, China, 2020, pp. 482-486.

[2] W. Tang, Y. Yuan, S. Xu, C. Sun and Z. Guo, ”5G NR Uplink Control Channel Coverage Enhancement Based on Sequence Segmented Detection with New Low-PAPR Sequences,” 2021 IEEE 21st International Conference on Communication Technology (ICCT), Tianjin, China, 2021, pp. 248-252.

[3] 3GPP, “Physical channels and modulation,” 3rd Generation Partnership Project (3GPP), TS 38.211 V 15.5.0, March. 2019.

[4] K. Kuchi, “Partial response DFT-precoded-OFDM modulation,” Transactions on Emerging Telecommunications Technologies, vol. 23, no. 7, pp. 632–645, May 2012.

[5] IITH et.al., “Comparison of pi/2 BPSK with and without frequency domain pulse shaping: Results with PA model,” 3GPP TSG-RAN WG1 Ad-Hoc NR Meeting, R1-1701180, Spokane, WA, USA, Jan. 16–20, 2017.

[6] Qualcomm, ”Lower PAPR reference signals”, 3GPP TSG RAN WG1 Meeting #94bis, R1-1811280, Chengdu, China, 8th - 12th October, 2018.

[7] IITH et.al., “ Low PAPR Reference Signals,” 3GPP TSG RAN WG1 AdHoc Meeting #1901, R1-1900215, Taipei, Taiwan, 21st – 25th January, 2019.

[8] M. S. A. Khan, K. Rao, S. Amuru and K. Kuchi, ”Low PAPR DMRS sequence Design for 5G-NR Uplink,” 2020 International Conference on COMmunication Systems & NETworkS (COMSNETS), Bengaluru, India, 2020, pp. 207-212.

[9] S. C. Thompson, A. U. Ahmed, J. G. Proakis, J. R. Zeidler, and M. J. Geile, “Constant Envelope OFDM,” IEEE Transactions on Communications, vol. 56, no. 8, pp. 1300–1312, Aug. 2008.

[10] T. F. Rahman, C. Sacchi, S. Morosi, A. Mazzinghi, and N. Bartolomei, “Constant-envelope multicarrier waveforms for millimeter wave 5G applications,” IEEE Trans. Veh. Technol., vol. 67, no. 10, pp. 9406–9420, 2018.

[11] G. Cui, C. Wang, W. Wang, and Y. Zhang, “Frequency offset compensation for satellite communication system with CE-OFDM,” China Commun., vol. 14, no. 8, pp. 93–104, 2017.

[12] A. U. Ahmed, S. C. Thompson, and J. R. Zeidler, “Channel estimation and equalization for CE-OFDM in multipath fading channels,” in MILCOM 2008, 2008, pp. 1–7.

[13] A. Sahin, E. Bala, R. Yang and R. L. Olesen, ”DFT-Spread OFDM with Frequency Domain Reference Symbols,” GLOBECOM 2017 - 2017 IEEE Global Communications Conference, Singapore, 2017, pp. 1-6.

[14] Yong Soo Cho, J. Kim, Won Young Yang, and C. G. Kang, MIMO-OFDM Wireless Communications with MATLAB. John Wiley & Sons, 2010.

[15] Y. Wang, Y. Xiao, L. Dan and H. Chen, ”On the BER Performance of Constant Envelope OFDM in Frequency Selective MIMO Channels With ML Detection,” in IEEE Wireless Communications Letters, vol. 12, no. 8, pp. 1354-1358, Aug. 2023.

[16] 3GPP. Evolved universal terrestrial radio access (E-UTRA); base station (BS) radio transmission and reception: 3GPP TS 36.104 version 8.6.0 release 8. Etsits, 2009.